Photoelectrochemical Water Splitting Using Concentrated Solar Flux Assisted $LaFeO_3$ Photocathode

M V N Surendra Gupta,[a,b] Hasan Baig, [c] K S Reddy,[d] Tapas K Mallick,[c] Bala Pesala,[a,b] and Asif A Tahir [*c]

[a]CSIR-Central Electronics Engineering Research Institute, Chennai, India.

[b]Academy of Scientific and Innovative Research, CSIR-SERC, Chennai, India

[c]Environmental and Sustainability Institute University of Exeter, Penryn, TR10 9FE, UK

[d]Indian Institute of Technology, Madras, Chennai, India.

ABSTRACT: Photoelectrochemical (PEC) water splitting by direct solar irradiation has been considered as a route to produce solar fuel but the technique is impede by limitation of the photocathode materials. Although $LaFeO_3$ photocathode has been identified as a potential candidate for spontaneous hydrogen generation with excellent stability, however lower current densities limit its photoelectrochemical performance. Using solar concentration could prove to be an effective method to leverage its performance. In this study, we have developed a strategy to improve the current density of $LaFeO_3$ photocathode by applying concentrated solar flux. The results demonstrate that the photocurrent density follows a linear relationship with flux concentration and 2-fold performance enhancement with 18 times of incident flux. Furthermore, the addition of H_2O_2 to the electrolyte solution has significantly improved the photocurrent induced by $LaFeO_3$ due to efficient scavenging of electrons. The fabricated $LaFeO_3$ photocathode is translucent and therefore a reflector element is placed behind the substrate to redirect light back to the photocathode. The incorporation of high flux concentration, scavenger and reflector element, enhanced current density by 9 times (to 0.872 mA/cm^2). Our results demonstrate that concentrated solar flux assisted $LaFeO_3$ photocathode will play a significant role in renewable hydrogen production and study will provide a direction to photoelectrochemical water splitting.

Keywords: Photoelectrochemical, water splitting, flux concentration, scavenger, reflector.

INTRODUCTION

According to BP energy outlook 2019, global energy demand will grow at an average rate of 1.2% annually [1]. A sizeable proportion of the energy consumed by anthropogenic activities is produced from fossil fuels leaving a carbon footprint. However, with the rapid depletion of fossil fuels, it is estimated that the known reserves will only last until the year 2112 at an economic growth rate of 1.5% [2]. Therefore, a substantial need for clean and conventional alternative energy sources is burgeoning. Of all the conventional sources, solar energy is clean, inexhaustible, abundant (430 quintillion Joules of energy/hour [3]) and renewable source of energy. Manifold technologies are available to harness solar radiation and convert to electricity and hydrogen, preeminent are photovoltaics [4], thin-film photovoltaics [5], wet-chemical photosynthesis [6] and photoelectrolysis. Viable technology among them is photoelectrolysis, combining photovoltaics and wet-chemical photosynthesis, to split the water by solar energy to produce hydrogen (with no emission of byproducts), which can be stored as a chemical fuel for after usage, as solar energy is intermittent.

Two prominent ways of water splitting are photocatalytic [7] and photoelectrochemical cells (PEC). Among them, PEC is the competent approach as it can absorb a greater fraction of solar energy by combining two different semiconductors. After the pioneering work of Honda and Fujishima in 1972 on photoelectrolysis using PEC cell [8], numerous semiconductor materials have been explored to develop stable and efficient PEC water splitting devices. Upon immersion of semiconductor in the electrolyte solution, majority charge carriers form a space charge layer [9] inside the electrode to equalize the Fermi levels to attain a thermodynamic equilibrium, forming Schottky-type electronic junction due to band bending. Besides, a Helmholtz layer, charged layer of opposite sign, is induced at the solid electrode surface. Under illumination, the valence electrons gain sufficient energy to break the bonding and inject into the conduction band, consequently creating electron-hole pairs. The photogenerated carriers generate photovoltage to drive the electrochemical reaction for solar to fuel production. Under standard illumination conditions, the minimum thermodynamic potential of 1.23 V is required (Gibbs free energy, ΔG = 237.2 kJ/mol) to convert one molecule of H_2O into H_2 and ½ O_2 [10]. In reality, due to thermodynamic losses (0.3 – 0.4 eV) and overpotentials (0.4 – 0.6 eV) [11] required for sluggish kinetics, the semiconductor needs to have a

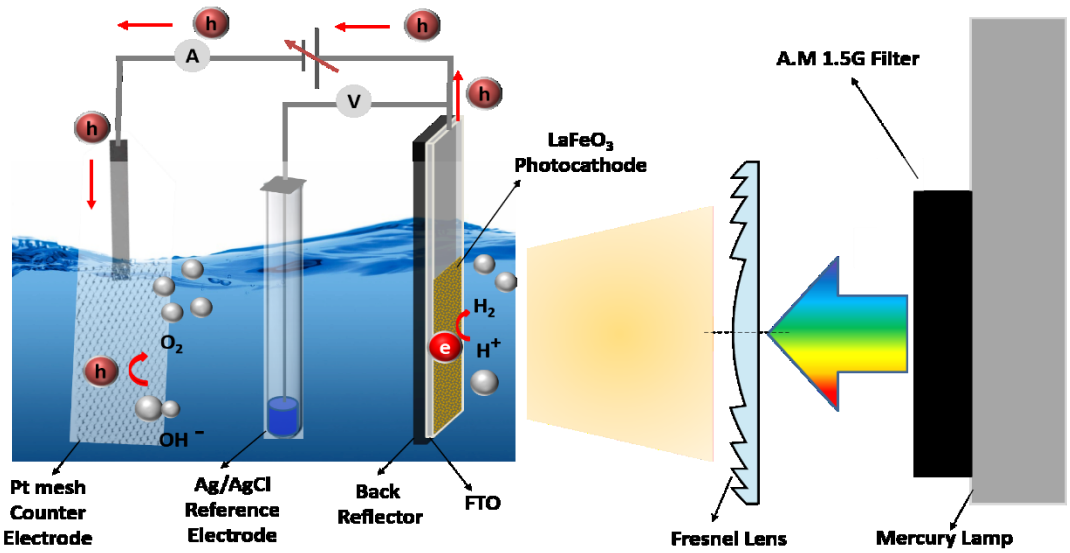

Figure 1:Schematic of experimental set-up. A 350 W high stability mercury (Hg) lamp with A.M 1.5G filter is used as a source for the experiments. Light from the filter is passed through the Fresnel lens to control the flux concentration of light incident upon th e $LaFeO_3$ photocathode film which is deposited on FTO substrate. A back reflector is used to reflect the light that is passing through the film and FTO substrate. Platinum mesh and Ag/AgCl are used as the counter and reference electrodes respectively.

minimum bandgap of 1.9 eV corresponds to the wavelength of 730 nm, below which the solar spectrum drops drastically [12]. Further, the semiconductor must be chemically stable in aqueous solution both in dark and under illumination. Another dominant factor that heeds is the band edge positions, in which the bottom level conduction band should be located above (more negative potential) the water reduction potential, $E^o(H+/H_2)$ and top level of valency band should be below (more positive potential) the water oxidation potential $E^o(H_2O/O_2)$.

Several materials have been explored since its inception in 1972 [8], in pursuit of optimal material for unassisted solar-driven water splitting. Single/Polycrystalline/thin film [13 - 14] TiO_2 has adequate stability, however the efficiency is less [15] due to its large bandgap (E_g = 3.2 eV). Other binary metal oxides having smaller bandgap such as α – Fe_2O_3 [16] and WO_3 [17] are extensively studied, yet their conduction band is below the water reduction potential, therefore an external bias potential is required. Ternary metal oxides such as $BiVO_4$[18], with an optimal bandgap (E_g = 2.4 eV) and a reasonable band edge for water redox reactions, has performance close to the thermodynamic maximum yet below the desired practical STH efficiency. Metal nitrides like Ta_3N_5 [19] and oxynitrides TaON [20] have been developed rapidly but they are not stable in aqueous medium leading to photo-corrosion and photo-oxidation.

Photocathodes which are p-type semiconductors such as GaP [21], Cu_2O [22] have been studied. GaP are not suitable for large scale applications while Cu_2O [E_g = 2.1 eV] has excellent properties for the solar hydrogen production as it cheap, abundant and favorable band positions but unstable under PEC condition and need to be protected with nanolayers of AZO (Al-doped Zinc oxide) to inhibit reduction of Cu_2O to Cu under illumination in aqueous electrolytes [23]. $CuFeO_2$, a copper-based ternary oxide has been an attractive material as it being stable under reductive conditions and is not easily degraded, however, its carrier generation needs further improvement [24]. Despite several p-type materials have been reported in PEC devices, they still suffer from low hydrogen evolution, longevity due to decline in photo-response. Latest p-type semiconductor $LaFeO_3$ has been developed with high photo-response and durability in aqueous reduction reactions [25]. Unbiased nanostructured $LaFeO_3$ photocathode has generated 0.18 μmol/cm^2 of hydrogen after 6 hours [26]. However, in [26], it was reported that the deposited $LaFeO_3$ films are thin and transparent leading to the low photocurrent. Therefore, new approaches that could enhance the performance beyond the existing ones are pursed-after.

In this work, we have explored four major entities that could potentially enhance the photocurrent of the $LaFeO_3$. They lineup as follows: 1) control on the thickness of the deposited film to arrive at absorption path length, a trade-off between high current density and bulk recombination of the separated charge carriers, 2) boosting the amount of solar flux radiation incident on the photocathode, 3) addition of H_2O_2 electron scavenger to improve

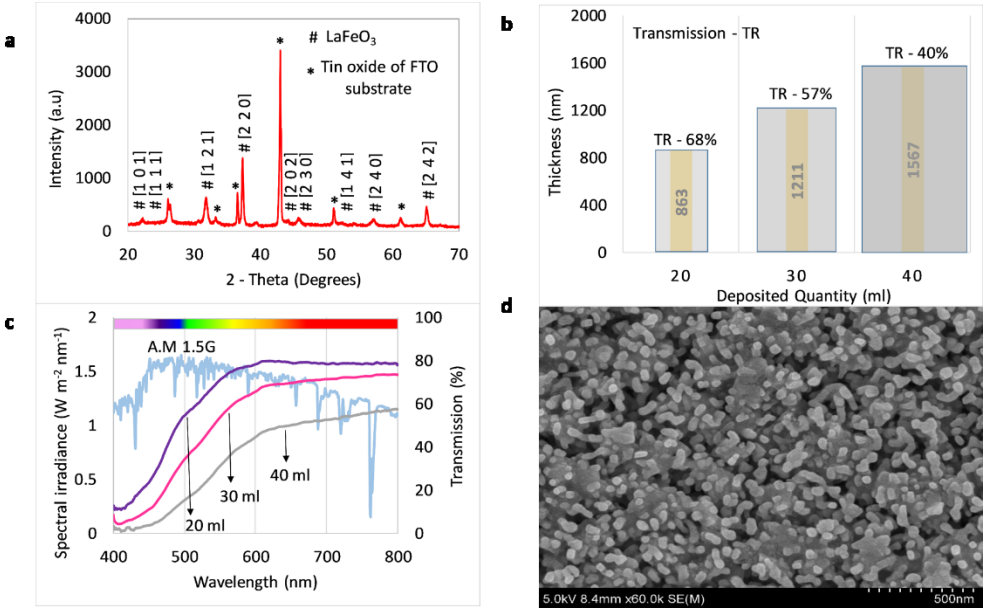

Figure 2: Material characterization of p-type $LaFeO_3$ photocathode. a, X-ray diffractogram of spray pyrolysis $LaFeO_3$ film deposited on FTO substrate after annealing at temperature of 550 ^oC for 3 hours. **b**, Thickness of films measured using surface profile are 863 nm, 1211 nm and 1567 nm for 20 ml, 30 ml and 40 ml of precursor sprayed respectively. The percentages on the top of each bar represents the average transmission of 68%, 57% and 40% for 20 ml, 30 ml and 40 ml respectively. **c,** Transmission spectrum of the three sample in the wavelength range of 400 – 800 nm measured using an in-house built optical characterization set-up **d**, Top view FESEM of $LaFeO_3$ thin film.

photocurrent induced by $LaFeO_3$ due to efficient scavenging of electrons, 4) back reflector element behind the substrate to redirect light back to the photoelectrode. The results demonstrate that the combination of these four factors has enhanced the performance of $LaFeO_3$ photocathode by 9 times compared to simple $LaFeO_3$ photocathode.

SYNTHESIS AND MATERIAL CHARACTERIZATION OF $LaFeO_3$ PHOTOCATHODE

Photocathode Preparation. Iron (III) nitrate nonahydrate (10 mmol) was dissolved in 25 ml methanol and 20 ml (35% solution) of aqueous ammonia (NH_3) was added. The solution was centrifuged at 2500 rpm for 15 min at 20 ^oC and the dark red colour precipitate was collected. The collected precipitate was washed twice with de-ionized water to eliminate the stench of ammonia. Lanthanum (III) iso-propoxide (10 mmol) was added to the precipitate along with 25 ml of methanol and 100 µl of Trifluoroacetic acid. The solution was stirred until it turned pellucid and then used for spray pyrolysis. Fluorine doped tin oxide (FTO) glass substrates are sequentially sonicated with ethanol, acetone and iso-propanol each of 15 min, rinsed with de-ionized water and dried with compressed air before spray pyrolysis. A cleaned substrate is placed on a hot plate at 150 ^oC. The precursor solution was taken into a 50 ml syringe, anchored onto syringe pump system and was sprayed at 1 ml/min assisted with compressed air through an ultrasonic atomizer nozzle (1 mm diameter), at a rate of 4.5 L/min. The precursor and compressed air are passed through vortex arrangement to generate aerosol for uniform deposition on to FTO substrate. Three samples are prepared by depositing 20 ml, 30 ml and 40 ml solution for 20 min, 30 min and 40 min respectively. Finally, the samples are annealed at 550 ^oC for 3 hours.

Material Characterization. XRD (Model: X'Pert Pro) is used to identify the phase purity and crystal structure of prepared $LaFeO_3$ films with a Cu Kα ($\lambda_{K\alpha}$ = 1.54060) radiation source of 40 kV at 30 mA. The diffraction data is collected in the range of 20^o – 70^o 2θ at a scan rate of 0.015^o/s. The XRD peak pattern is shown in Fig. 2a which confirms the presence of $LaFeO_3$ indexed to orthorhombic system (JCPDS 00-037-1493) preferentially oriented in [2 2 0] direction and tin oxide rutile phases (JCPDS 01-079-6887) from the film and FTO substrate respectively. Three samples are prepared with a deposited precursor solution of 20 ml, 30 ml and 40 ml. The thickness of the samples is measured using 3-D noncontact surface profiler using step-technique and the obtained thickness is 863 nm, 1211 nm and 1567 nm for the sample 20 ml, 30 ml and 40 ml respectively as shown in Fig. 2b. The deposited films are translucent, and the normalized transmission spectrum is shown in Fig. 2c. The average transmission percentage

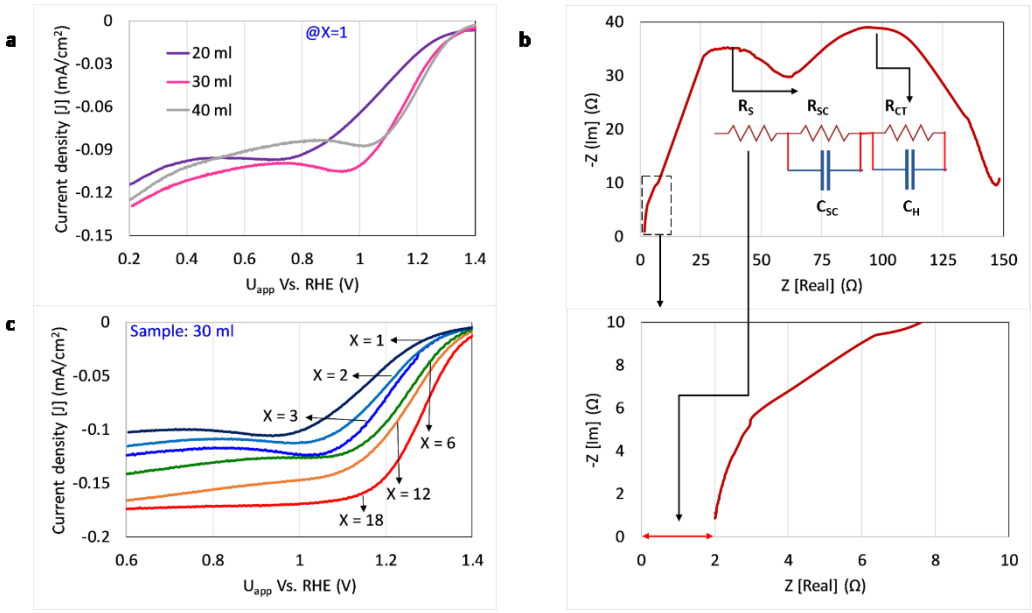

Figure 3: Photoelectrochemical analysis in three electrode voltammetry system. a, Comparison of current density versus applied potential curves measured at X=1 illumination for the three samples 20 ml (863 nm), 30 ml (1211 nm) and 40 ml (1567 nm). **b,** Nyquist plot of EIS measurements carried out for $LaFeO_3$ in 0.1 M NaOH solution at an electrode potential of 1.45 V vs. RHE for 30 ml sample. The equivalent circuit model was fitted using Z-Fit function of E-C Lab software. R_s is the uncompensated series resistance, arising due to the FTO and the conductivity of ions in the electrolyte and external wire resistance. The below expanded figure of dotted area shows the series resistance as 2.0 Ω, where the Nyquist plot begins. **c,** Current density versus applied potential curves measured at various flux concentrations ranging from X = 1 (dark blue curve) to X = 18 (red curve) for the optimized thickness of the sample 30 ml (1211 nm).

measured over the wavelength range of 400 – 800 nm is 67% (20 ml), 58% (30 ml) and 40% (40 ml). With an increase in the thickness of the film, the percentage of average transmission has decreased implying that the amount of light absorbed by the film has increased. FESEM image of the $LaFeO_3$ photoelectrode film shown in Fig. 2d has a uniform coral-like structure with well-connected crystal grains. The elemental analysis is carried out using energy-dispersive x-ray spectroscopy (EDS) (Fig. S1)

RESULTS AND DISCUSSION

Photoelectrochemical Measurements. To analyze the performance of the $LaFeO_3$ photocathode, PEC measurements were carried out in conventional three-electrode voltammetry system (saturated Ag/AgCl as a reference electrode, platinum mesh as counter electrode and $LaFeO_3$ as a working electrode) performed in dark and under illumination to obtain the photo-response of the working electrode. Linear sweep voltammetry measurements were carried out by sweeping current-potential scans in 0.1 M NaOH electrolyte (pH 13) with scanning direction from cathodic to anodic potentials at a scan rate of 10 mV/s. The three-electrode wires are wired to a potentiostat (SP 200, Biologic Science Instrument) operated by Autolab software. Fig. 3a shows PEC performance of the $LaFeO_3$ films deposited with different thickness of 863 nm, 1211 nm and 1567 nm under 1 sun (X=1) illumination. Sample (20 ml) has exhibited a lower photocurrent response due to a lower thickness of 863 nm leading to limited photon absorption. Sample (30 ml) with the thickness of 1211 nm, PEC performance was enhanced, as thicker films create a greater number of electron and hole pairs due to absorption of a greater number of photons. Sample (40 ml), with the thickness of 1567 nm higher than 30 ml sample thickness (1211 nm), the photocurrent has decreased as the charge carriers are hampered due to long diffusion distance for their facile transfer to the surface before recombination.

Nernst equation [1] [27] is used to convert the voltammetric data collected using Ag/AgCl reference electrode to reversible hydrogen electrode

$$E_{RHE} = E_{Ag/AgCl} + 0.059 * pH + E^{o}_{Ag/AgCl} \qquad (1)$$

where E_{RHE} is the converted potential, $E^{o}_{Ag/Agcl}$ = 0.197 at 25° C and $E_{Ag/Agcl}$ is the working potential.

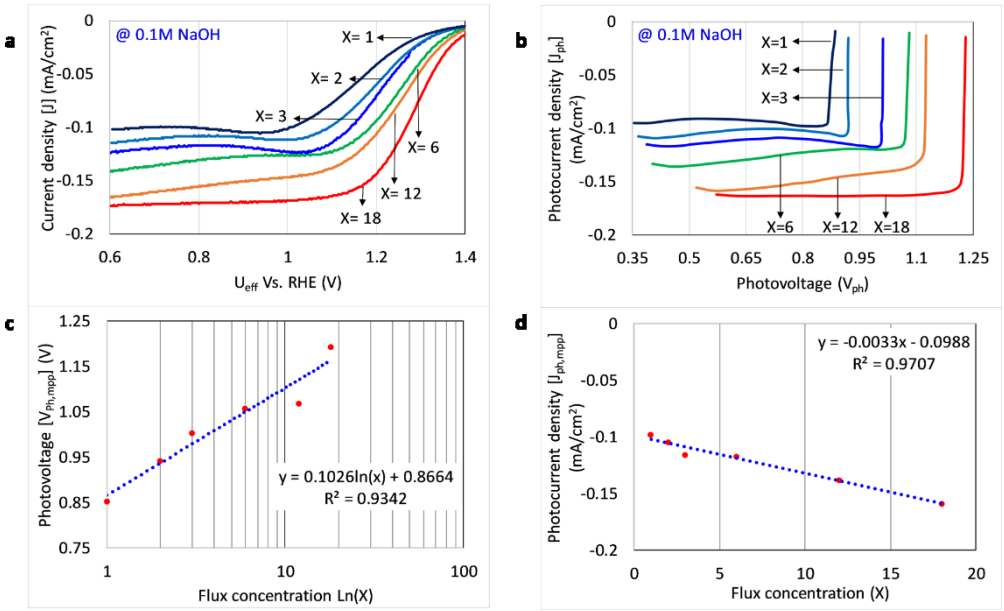

Figure 4: Intrinsic photovoltaic properties of $LaFeO_3$ photocathode. a, Compensated current density versus applied potential curves obtained for the sample (30 ml) measured under concentration ranging from X = 1 (dark blue curve) to X = 18 (red curve). **b,** Photocurrent density versus calculated photovoltage for various flux concentrations from which the maximum power point is extracted. **c,** Photovoltage at the maximum power point as a function of flux concentration having logarithmic relationship. **d,** Photocurrent current density at the maximum power point as a function of flux concentration having linear relationship.

The electrical behaviour of the photocathode/electrolyte interface is obtained by electrochemical impedance spectroscopy (EIS). EIS measurements are performed for 30 ml sample using a three-electrode configuration under the dark condition at a fixed potential of 1.45 V Vs. RHE in 0.1M NaOH solution in the frequency range of 1 MHz – 10 Hz with modulating signal magnitude of 10 mV. The measurements are carried out at 1.45 V as almost no current is drawn through the reference electrode since high impedance is observed in the device. The obtained EIS spectrum is shown in Fig. 3b having two semi-circles. The Nyquist plot of EIS spectra was fitted to the electrical analogue using Z-Fit function of E-C Lab software. The equivalent circuit shows a resistance (R_S) in series with two RC elements. R_S is the series resistance which includes FTO resistance and the contact resistance. The dotted area in Fig. 3b is expanded and shown below it. The red arrow represents the series resistance which is 2.0 Ω. The first RC element (R_{SC} and C_{SC}) represents semiconductor bulk and the second RC element (R_{CT} and C_H) represents surface phenomena [28].

Thrust for exploring the solar flux concentration comes from concentrated photovoltaics (CPV), where there is an incremental power conversion with a boost in the irradiation. Only a few studies have been conducted to understand the effect of solar flux concentration on the efficacy of the photoelectrochemical cells (PEC) for water splitting applications. Earliest studies on α–Fe_2O_3 are conducted by Klahr and Hamann [29], the slope of the photocurrent density increases with increase in the light intensity, however, the flux concentration is in the range 0.35 – 3.9 suns. A photocathode (p-GaInP2) paired with hematite and tungsten trioxide photoanodes was illuminated with 1 W/cm^2 (10 suns), despite resulted in very low current densities [30]. Recent studies on hematite (with dopants Ti and Si) was carried out at high flux concentrations ranging from 1 to 25 suns, elucidates the linear behavior of the water photo-oxidation current density with light intensity and concomitantly photovoltage scales with logarithmic behaviour [31]. Therefore, reported studies explicate with light a control parameter, pitch towards charge transfer in a battle between the recombination rate and charge transfer [32].

Incident Flux Concentration Calibration. In our measurements, the solar flux concentration was controlled by adjusting the distance between the Fresnel lens and PEC cell to avoid any concurrent changes in the incident spectrum. The lens used in this study is a typical square

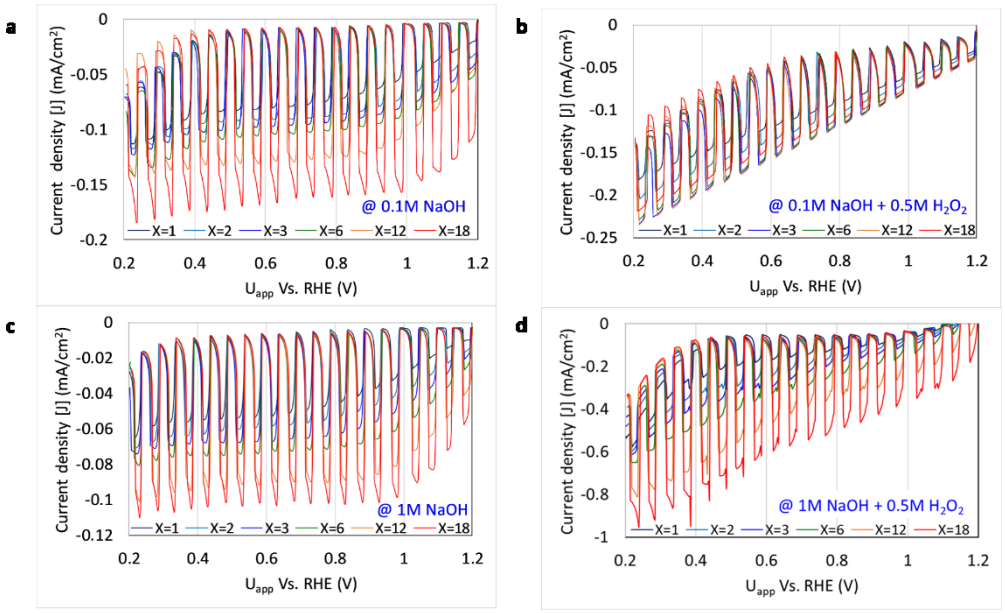

Figure 5: Chopped-light voltammetry measurements under concentrations ranging from X=1 (dark blue curve) to X=18 (red curve). a, In 0.1M NaOH solution. **b,** In 0.1M NaOH + 0.5M H_2O_2 solution. **c,** In 0.1M NaOH solution. **d,** In 0.1M NaOH + 0.5M H_2O_2 solution

Fresnel lens made of PMMA with an effective area of 130 x 130 mm^2 and a focal distance of 152 mm. Its thickness is 1.8 mm and the ring facet spacing is 0.381 mm with F-number of 0.83 [33]. Initially, a photovoltaic cell (PV) of 10 x 10 mm^2 is taken and placed under AAA class solar simulator. The measured short circuit current of the PV cell is 38 mA under 1 sun illumination. Next, to find out the PEC cell position and the flux concentration, PV cell is sandwiched between thin microscopic slides to isolate from the electrolyte and placed inside the solution. A 350 W high stability mercury (Hg) lamp with AM 1.5 filter is used to mimic the solar spectrum and by controlling the distance the short circuit current is measured to calibrate the flux concentration.

The optimal thickness for which higher photocurrent density response observed was 30 ml sample as shown in Fig. 3a. For this sample, the PEC performance is explored under a wide range of solar flux concentrations. As shown in Fig. 1, the solar flux concentration was controlled by adjusting the distance between the Fresnel lens and PEC cell to avoid any concurrent changes in the incident spectrum. A solar cell is used to calibrate the flux concentration with distance by measuring its short circuit current (Fig. S5). Fig. 3c expounds the role of incident light concentration on the current density of $LaFeO_3$ photocathode. For an applied voltage of U_{app} at 1.0 Vs. RHE, the current density is 0.101 mA/cm^2 and 0.169 mA/cm^2 at X=1 and X=18 concentrations respectively. This clearly demonstrates as the solar flux concentration has increased from the lowest (X=1) to highest (X=18), the current density has increased by 70%. Though the performance of photocathode film is not similar to the conventional solar cells of current being proportional to flux concentration, it still showed a significant improvement in the current density.

Intrinsic Photovoltaic Properties of LaFeO3 Photocathode. The measured dark current has a steep slope at higher current values, and this arises due to the series resistance (R_s) obtained from the Nyquist plot of EIS spectra (Fig. S3). Therefore, the actual effective potential at the working electrode is calculated from equation [2]:

$$U_{eff} = U_{app} - IR_s \quad (2)$$

where U_{app} is the applied potential I is the measured current and series resistance, Rs = 2.0 Ω.

Therefore, the compensated curves obtained with the potential correction is shown in Fig. 4a. To further explore the performance of the $LaFeO_3$ photocathode, the intrinsic photovoltaic properties, photovoltage and photocurrent density are obtained from compensated curves using the approach reported in ref [34] (Fig. S2). Fig. 4b shows the photocurrent density for the calculated photovoltage under various flux concentrations. The flux concentration has increased only till X=18, as the bubbles start to appear at higher currents at the counter electrode, beyond which provides noisy data. Similar to the approach in photovoltaics for the calculation of maximum power,

here the product where photovoltage (V_{ph}) x photocurrent (J_{ph}) is maximal is obtained from the curves in Fig. 4b. The

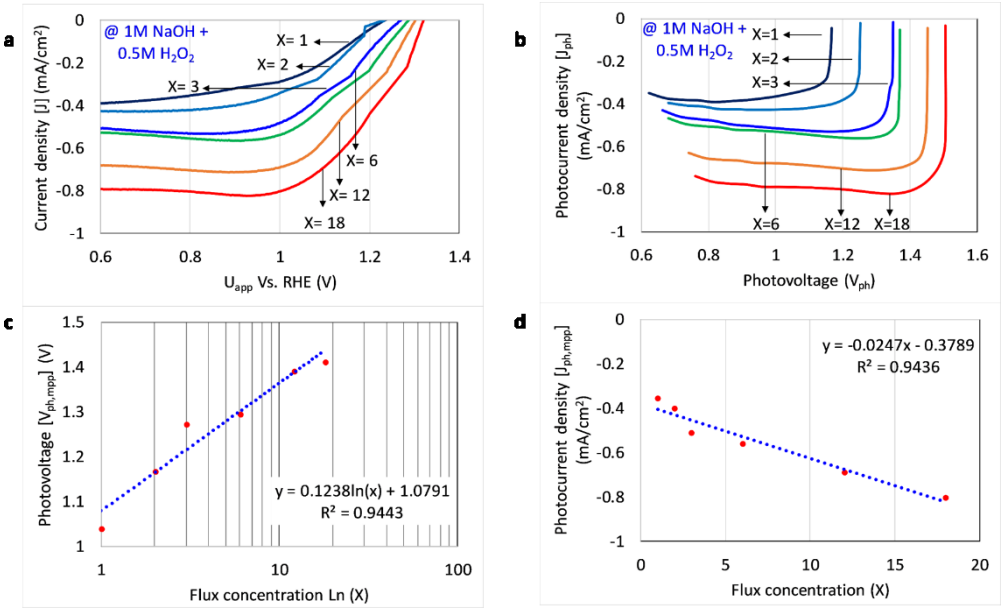

Figure 6: Intrinsic photovoltaic properties of $LaFeO_3$ photocathode with H_2O_2 scavenger. a, Current density versus applied potential curves measured at various flux concentrations ranging from X = 1 (dark blue curve) to X = 18 (red curve) for the optimized thickness of the sample 30 ml (1211 nm). **b,** Photocurrent density versus calculated photovoltage for various flux concentrations from which the maximum power point is extracted. **c,** Photovoltage at the maximum power point as a function of flux concentration having logarithmic relationship. **d,** Photocurrent current density at the maximum power point as a function of flux concentration having linear relationship.

extracted photovoltage at maximum power point (MPP), $V_{ph,mpp}$ and the flux concentration is shown in Fig. 4c. It is noticeable that photovoltage at the maximum power point has a logarithmic relationship as a function of flux concentration with a slope of 243 mV per decade and dashed trend line gives the best logarithmic fit with $V_{ph,mpp} = 0.1026\ln(X) + 0.8664$ and $R^2 = 0.9342$, infer that with concentration the maximum power point shifts to higher photovoltages. While the photocurrent density thought not proportional, yet has a linear relationship with concentration and the dashed trend line gives the best linear fit with $J_{ph,mpp} = -0.0033X - 0.0988$ and $R^2 = 0.9707$.

Electron Scavenger. Electron scavengers like hydrogen peroxide (H_2O_2) and sodium persulfate ($Na_2S_2O_8$) have been explored to improve the charge transfer kinetics [35 -36]. In this study, we have added H_2O_2 to the NaOH electrolyte solution. Fig. 5 shows the chopped-light voltammetry measurements under various incident light concentrations ranging from X=1 to X=18. Fig. 5a shows the chopped measurements in 0.1M NaOH solution. It can be observed as the voltage sweep is moving more towards anodic potentials, negative current transients are appeared upon switching on of the light which represents the accumulation of electrons at the electrode/electrolyte interface without injection to the electrolyte. Therefore, this shows that semiconductor/electrolyte systems have high injection barrier characteristics. Upon addition of 0.5M H_2O_2 solution to the NaOH electrolyte, these transient negative current peaks have disappeared which can be observed from Fig. 5b and only Faradic photocurrents were observed in the entire sweep potential. Therefore, it indicates that all the electrons that reach the electrode/electrolyte interface contribute to the water reduction reaction and removes the injection barrier that was observed in the 0.1M NaOH solution. From Fig. 5a to Fig. 5b, we observe that the photocurrents measured in both electrolyte solution converge at lower potentials, but there is no doubling in current. However, it is reported [37] that in some p-type semiconductor current doubling can occur according to the equation [3]:

$$H_2O_2 + 2H^+ + e^- \rightarrow OH^- + OH^* + 2H^+ \rightarrow 2H_2O + h^+ \quad (3)$$

Therefore, we have increased the molarity of NaOH solution from 0.1M to 1M by adding the same amount of 0.5M H_2O_2 solution to the electrolyte. Again, the chopped-light voltammetry measurements were carried out and a significant improvement in the current density is observed for all concentrations as shown in Fig. 5d with no transient negative current peaks. However, at very low voltages below 0.6 V Vs. RHE minor peaks appear. In 1M NaOH solution more OH^- ions are present and that favors the forward reaction when H_2O_2 is added to it.

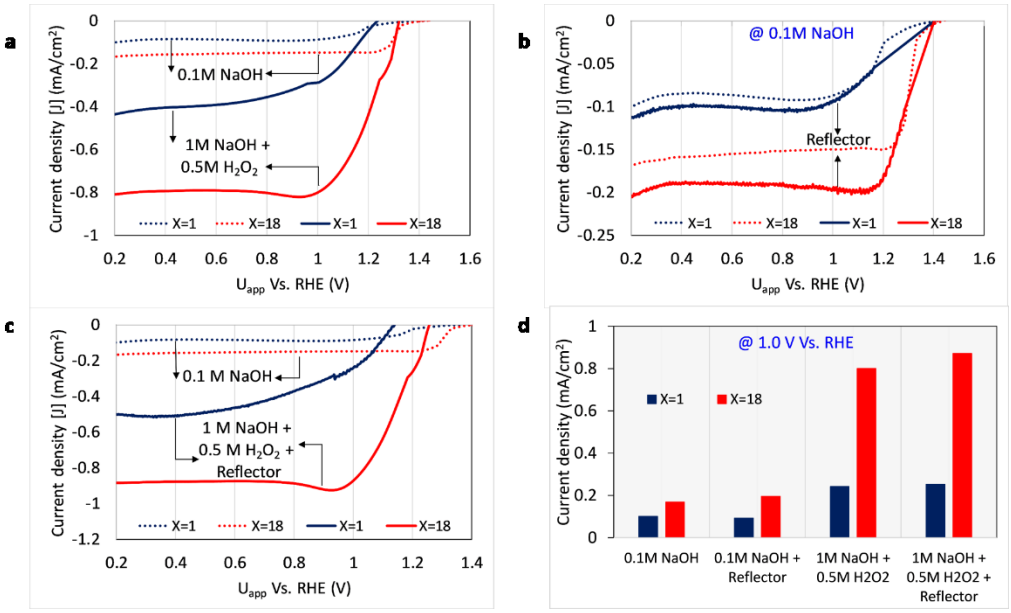

Figure 7: Overall enhancement of $LaFeO_3$ photocathode. a, LSV measurements in 0.1M NaOH and 1M NaOH + 0.5 M H_2O_2 electrolyte solutions at X=1 and X=18. **b,** LSV measurements in 0.1M NaOH electrolyte solution with and without reflector element at X=1 and X=18. **c,** LSV measurements in 0.1M NaOH (no reflector) with 1M NaOH + 0.5M H_2O_2 (with reflector) electrolyte solution at X=1 and X=18. **d,** Comparison of all current densities at 1.0 V Vs. RHE in 0.1M NaOH and 1M NaOH + 0.5M H_2O_2 electrolyte solutions with and without the reflector element at X=1 and X=18.

Fig. 6a shows the current density curves for with respect to the applied potential curves for various incident light concentrations in 1M NaOH + 0.5M H_2O_2 solution. It can be observed at an applied potential of 1.0 V Vs. RHE, the current density at X=18 is 0.80 mA/cm^2 which is more than 4 times the current density observed in 0.1M NaOH solution of 0.169 mA/cm^2. The same approach as followed above was used to determine the intrinsic photovoltaic characteristics of $LaFeO_3$ photocathode with H_2O_2 scavenger solution and the photocurrent density with respect to the calculated photovoltage was shown in Fig. 6b. The extracted photovoltage at the maximum power point has a logarithmic relationship with flux concentration as shown in Fig. 6c with a slope of 281 mV per decade and fit equation of $V_{ph,mpp} = 0.1238\ln(X) + 1.0791$ and $R^2 = 0.9443$. Further, the photocurrent density has a linear relationship with flux concentration with fit equation of $J_{ph,mpp} = -0.0247X - 0.3789$ and $R^2 = 0.9436$.

Overall Enhancement With Reflector Element. As mentioned, the fabricated samples are translucent, therefore the optimized 30 ml sample has an average transmission percentage of 57%. In-house built optical set-up is shown in Fig. S4. Therefore, a reflector is placed behind the sample to reflect the transmitted light. The reflector has an average reflectance of 94% in the spectral range of 300 – 1200 nm [38]. Fig. 7b shows the LSV measurements obtained with reflector element in 0.1M NaOH solution at concentrations X=1 and X=18. It can be observed that the current density is improved by approximately 10% due to the reflector element. Further, we have carried out LSV measurements in 1M NaOH + 0.5M H_2O_2 solution with reflector element as shown in Fig. 7c at X=1 and X=18 concentrations. In comparison to the LSV measurements carried out without reflector element as shown in Fig. 7a, the proportional improvement of 10% is observed from Fig. 7c in 1M NaOH + 0.5M H_2O_2 due to reflector. Finally, in Fig. 7d, the current density at 1.0 V Vs. RHE is shown for all the four different configurations at X=1 and X=18 concentrations. It can be observed that there is a significant improvement in the performance of $LaFeO_3$ photocathode from first configuration of 0.1M NaOH electrolyte at X=1 concentration (0.101 mA/cm^2) to last configuration of 1M NaOH solution + 0.5M H_2O_2 + Reflector at X=18 concentration (0.872 mA/cm^2).

CONCLUSIONS

In summary, we have explored four entities: optimal thickness, flux concentration, electron scavenger and reflector element to enhance the current density of the $LaFeO_3$ photocathode. On comparing the current density measurements for all the four entities for the optimal thickness sample (30 ml - 1211 nm) at 1.0 V vs. RHE, the current density under 1 sun illumination in 0.1 M NaOH solution has a current density of 0.101 mA/cm^2, at 18 sun concentration in 0.1 M NaOH solution has a current

density of 0.169 mA/cm^2, in H_2O_2 electron scavenger solution (1M NaOH + 0.5M H_2O_2) under 18 sun illumination has a current density of 0.800 mA/cm^2 and finally with a reflector under 18 sun illumination in 1M NaOH + 0.5M H_2O_2 has a current density of 0.872 mA/cm^2. It is evident that there is 9 times increment in the current density from 0.101 mA/cm^2 to 0.872 mA/cm^2 with all the techniques discussed in the paper. we observe that though the relation between the flux concentration and the current density is linear, the current obtained is not proportional and can be explored further. we believe that the current work has provide a new strategy to improve the performance of photoelectrode for PEC solar hydrogen production.

ASSOCIATED CONTENT

Supporting Information

EDS spectrum of $LaFeO_3$ photocathode, the procedure to obtain photovoltage and photocurrent, Dark voltammetry measurements, optical characterization set-up, Flux concentration calibration, on-set voltage, maximum power, temperature increase estimation, ideality factor.

AUTHOR INFORMATION

Corresponding Author

*A.Tahir@exeter.ac.uk

Notes

The authors declare no competing financial interest.

ACKNOWLEDGEMENTS

Author M.V.N.S.G acknowledges the SRF fellowship provided by CSIR. We also acknowledge UKIERI-DST 2016-17-0089 project. This work has been conducted as part of the research project "Joint UK-India Clean Energy Centre (JUICE)" which is funded by the RCUK Energy Programme (contract no: EP/P003605/1)

REFERENCES

1. BP (2019) Statistical Review of World Energy, June 2019.
2. Stephens E, Ross IL, Mussgnug JH, Wagner LD, Borowitzka MA, Posten C, Kruse O, Hankamer B. Future prospects of microalgal biofuel production systems. Trends in plant science. 2010 Oct 1;15(10):554-64.
3. Basic Research Needs for Solar Energy Utilization; Lewis, N. S., Crabtree, G., Eds.; Office of Science, U. S. Department of Energy: Washington, DC, 2005
4. van de Krol R, Liang Y, Schoonman J. Solar hydrogen production with nanostructured metal oxides. Journal of Materials Chemistry. 2008;18(20):2311-20.
5. Atwater HA, Polman A. Plasmonics for improved photovoltaic devices. InMaterials For Sustainable Energy: A Collection of Peer-Reviewed Research and Review Articles from Nature Publishing Group 2011 (pp. 1-11).
6. Kuang T. A breakthrough of artificial photosynthesis. National Science Review. 2016 Mar 1;3(1):2-3.
7. Fu S, Song J, Zhu C, Xu GL, Amine K, Sun C, Li X, Engelhard MH, Du D, Lin Y. Ultrafine and highly disordered Ni2Fe1 nanofoams enabled highly efficient oxygen evolution reaction in alkaline electrolyte. Nano Energy. 2018 Feb 1;44:319-26.
8. Fujishima A, Honda K. Electrochemical photolysis of water at a semiconductor electrode. nature. 1972 Jul;238(5358):37-8.
9. Nozik AJ. Photoelectrochemistry: applications to solar energy conversion. Annual review of physical chemistry. 1978 Oct;29(1):189-222.
10. Ager JW, Shaner MR, Walczak KA, Sharp ID, Ardo S. Experimental demonstrations of spontaneous, solar-driven photoelectrochemical water splitting. Energy & Environmental Science. 2015;8(10):2811-24.
11. Van de Krol R, Grätzel M. Photoelectrochemical hydrogen production. New York: Springer; 2012.
12. Chen HM, Chen CK, Liu RS, Zhang L, Zhang J, Wilkinson DP. Nano-architecture and material designs for water splitting photoelectrodes. Chemical Society Reviews. 2012;41(17):5654-71.
13. Nowotny J, Bak T, Nowotny MK, Sheppard LR. Titanium dioxide for solar-hydrogen I. Functional properties. International journal of hydrogen energy. 2007 Sep 1;32(14):2609-29.
14. Grimes CA, Varghese OK, Ranjan S. Oxide Semiconductors Nano-Crystalline Tubular and Porous Systems. InLight, Water, Hydrogen 2008 (pp. 257-369). Springer, Boston, MA.
15. Murphy AB, Barnes PR, Randeniya LK, Plumb IC, Grey IE, Horne MD, Glasscock JA. Efficiency of solar water splitting using semiconductor electrodes. International journal of hydrogen energy. 2006 Nov 1;31(14):1999-2017.
16. Dias P, Vilanova A, Lopes T, Andrade L, Mendes A. Extremely stable bare hematite photoanode for solar water splitting. Nano Energy. 2016 May 1;23:70-9.
17. Solarska R, Jurczakowski R, Augustynski J. A highly stable, efficient visible-light driven water photoelectrolysis system using a nanocrystalline WO 3

photoanode and a methane sulfonic acid electrolyte. Nanoscale. 2012;4(5):1553-6.
18. Pihosh Y, Turkevych I, Mawatari K, Uemura J, Kazoe Y, Kosar S, Makita K, Sugaya T, Matsui T, Fujita D, Tosa M. Photocatalytic generation of hydrogen by core-shell WO 3/BiVO 4 nanorods with ultimate water splitting efficiency. Scientific reports. 2015 Jun 8;5:11141.
19. Li Y, Takata T, Cha D, Takanabe K, Minegishi T, Kubota J, Domen K. Vertically aligned Ta3N5 nanorod arrays for solar- driven photoelectrochemical water splitting. Advanced materials. 2013 Jan 4;25(1):125-31.
20. Higashi M, Domen K, Abe R. Highly stable water splitting on oxynitride TaON photoanode system under visible light irradiation. Journal of the American Chemical Society. 2012 Apr 25;134(16):6968-71.
21. Memming R, Schwandt G. Electrochemical properties of gallium phosphide in aqueous solutions. Electrochimica Acta. 1968 Jun 1;13(6):1299-310.
22. Meyer BK, Polity A, Reppin D, Becker M, Hering P, Klar PJ, Sander T, Reindl C, Benz J, Eickhoff M, Heiliger C. Binary copper oxide semiconductors: From materials towards devices. physica status solidi (b). 2012 Aug;249(8):1487-509.
23. Paracchino A, Laporte V, Sivula K, Grätzel M, Thimsen E. Highly active oxide photocathode for photoelectrochemical water reduction. Nature materials. 2011 Jun;10(6):456-61.
24. Sivula K, Van De Krol R. Semiconducting materials for photoelectrochemical energy conversion. Nature Reviews Materials. 2016 Feb;1(2):15010.
25. Yu Q, Meng X, Wang T, Li P, Liu L, Chang K, Liu G, Ye J. A highly durable p-LaFeO 3/n-Fe 2 O 3 photocell for effective water splitting under visible light. Chemical communications. 2015;51(17):3630-3.
26. Pawar GS, Tahir AA. Unbiased spontaneous solar fuel production using stable LaFeO 3 photoelectrode. Scientific reports. 2018 Feb 22;8(1):1-9.
27. Gómez-Solís C, Ballesteros JC, Torres-Martínez LM, Juárez-Ramírez I. RuO2–NaTaO3 heterostructure for its application in photoelectrochemical water splitting under simulated sunlight illumination. Fuel. 2016 Feb 15;166:36-41.
28. Lopes T, Andrade L, Le Formal F, Gratzel M, Sivula K, Mendes A. Hematite photoelectrodes for water splitting: evaluation of the role of film thickness by impedance spectroscopy. Physical Chemistry Chemical Physics. 2014;16(31):16515-23.
29. Klahr BM, Hamann TW. Voltage dependent photocurrent of thin film hematite electrodes. Applied Physics Letters. 2011 Aug 8;99(6):063508.
30. Wang H, Deutsch T, Turner JA. Direct water splitting under visible light with a nanostructured photoanode and GaInP2 photocathode. ECS Transactions. 2008 Jan 15;6(17):37.
31. Segev G, Dotan H, Malviya KD, Kay A, Mayer MT, Grätzel M, Rothschild A. High Solar Flux Concentration Water Splitting with Hematite (α-Fe2O3) Photoanodes. Advanced Energy Materials. 2016 Jan;6(1):1500817.
32. Wijayantha KU, Saremi-Yarahmadi S, Peter LM. Kinetics of oxygen evolution at α-Fe 2 O 3 photoanodes: a study by photoelectrochemical impedance spectroscopy. Physical chemistry chemical physics. 2011;13(12):5264-70.
33. Ferrer-Rodríguez JP, Baig H, Fernández EF, Almonacid F, Mallick T, Pérez-Higueras P. Optical modeling of four Fresnel-based high-CPV units. Solar Energy. 2017 Oct 1;155:805-15.
34. Dotan H, Mathews N, Hisatomi T, Grätzel M, Rothschild A. On the solar to hydrogen conversion efficiency of photoelectrodes for water splitting.The Journal of Physical Chemistry Letters. 2014;5(19):3330-3334.
35. Dotan H, Sivula K, Grätzel M, Rothschild A, Warren SC. Probing the photoelectrochemical properties of hematite (α-Fe 2 O 3) electrodes using hydrogen peroxide as a hole scavenger. Energy & Environmental Science. 2011;4(3):958-64.
36. Maijenburg AW, Zoontjes MG, Mul G. Insight into the origin of the limited activity and stability of p-Cu2O films in photoelectrochemical proton reduction. Electrochimica acta. 2017 Aug 10;245:259-67.
37. Minks BP, Vanmaekelbergh D, Kelly JJ. Current-doubling, chemical etching and the mechanism of two-electron reduction reactions at GaAs: Part 2. A unified model. Journal of electroanalytical chemistry and interfacial electrochemistry. 1989 Nov 24;273(1-2):133-45.
38. Baig H, Montecucco A, Siviter J, Li W, Paul M, Sweet T, Gao M, Mullen PA, Marai EA, Knox AR, Mallick T. Indoor characterization of a reflective type 3D LCPV system. InAIP Conference Proceedings 2016 Sep 1 (Vol. 1766, No. 1, p. 020002). AIP Publishing LLC.